Adaptive space-time multiresolution techniques for nonlinear PDEs

Kai Schneider

M2P2-CNRS & CMI, Université de Provence, Marseille, France

Joint work with : Margarete Domingues, INPE, Brazil
Sonia Gomes, Campinas, Brazil
Olivier Roussel, TCP, Unversität Karlsruhe, Germany

1ères journées du GDR Calcul
9-10 November 2009, Institut Henri Poincaré, Paris, France

Outline

- Motivation
- Introduction
- Adaptivity in space and time
- Adaptive multiresolution method
- Local time stepping / Controlled time stepping
- Applications to reaction-diffusion equations
- Applications to compressible Euler and Navier-Stokes
- Conclusions and perspectives

Motivation

Context: Systems of nonlinear partial differential equations (PDEs) of hyperbolic or parabolic type.

Turbulent reactive or non-reactive flows exhibit a multitude of active spatial and temporal scales.

Scales are mostly not uniformly distributed in the space-time domain,

Efficient numerical discretizations could take advantage of this property -> adaptivity in space and time

Reduction of the computational complexity with respect to uniform discretizations

while controlling the accuracy of the adaptive discretization.

Here: adaptive multiresolution techniques

Introduction

- **Multiresolution schemes** (Harten 1995)
  - Solution on fine grid -> solution on coarse grid + details
  - Details “small” -> interpolation, no computation (CPU time reduced)
  - 2d non-linear hyperbolic problems (Bihari-Harten 1996, Abgrall-Harten 1996, Chiavassa-Donat 2001, Dahmen et al. 2001, …)

- **Adaptive Multiresolution schemes**
  (Müller 2001, Cohen et al. 2002, Roussel et al. 2003, Bürger et al. 2007, …)

  - Details “small” -> interpolation and remove from memory (CPU time and memory reduction)

- **Aim of this talk**
  - fully adaptive schemes (space + time) for 2d and 3d problems
  - Compare with Adaptive Mesh Refinement (preliminary results)

Adaptivity: space and time

Numerical method: finite volume schemes

Space adaptivity (MR): Harten's multiresolution (MR) for cell averages.
Decay of the wavelet coeffcients to obtain information on local regularity of the solution.
coarser grids in regions where coeffcients are small and the solution is smooth,
while fine grids where coeffcients are significant and the solution has strong variations.

Controlled Time Stepping (CTS): The time integration with variable time steps,
time step size selection is based on estimated local truncation errors.
When the estimated local error is smaller than a given tolerance, the time step is increased to
make the integration more effcient.

Local time stepping (LTS): Scale-dependent time steps. Different time steps, according to each cell scale: if Δt is used for the cells in the finest level, then a double time step $2\Delta t$ is used in coarser level with double spacing.
Required missing values in ghost cells are interpolated in intermediate time levels.

Harten multiresolution

Nested dyadic grids $\Omega = (\Omega_{l,i})_{0 \leq i < 2^l}$, $0 \leq l \leq L$

Data: Cell-average value on $\Omega_{l,i}$: $\bar{U}_{l,i} = \dfrac{1}{|\Omega_{l,i}|} \displaystyle\int_{\Omega_{l,i}} U \, d\mathcal{V}$

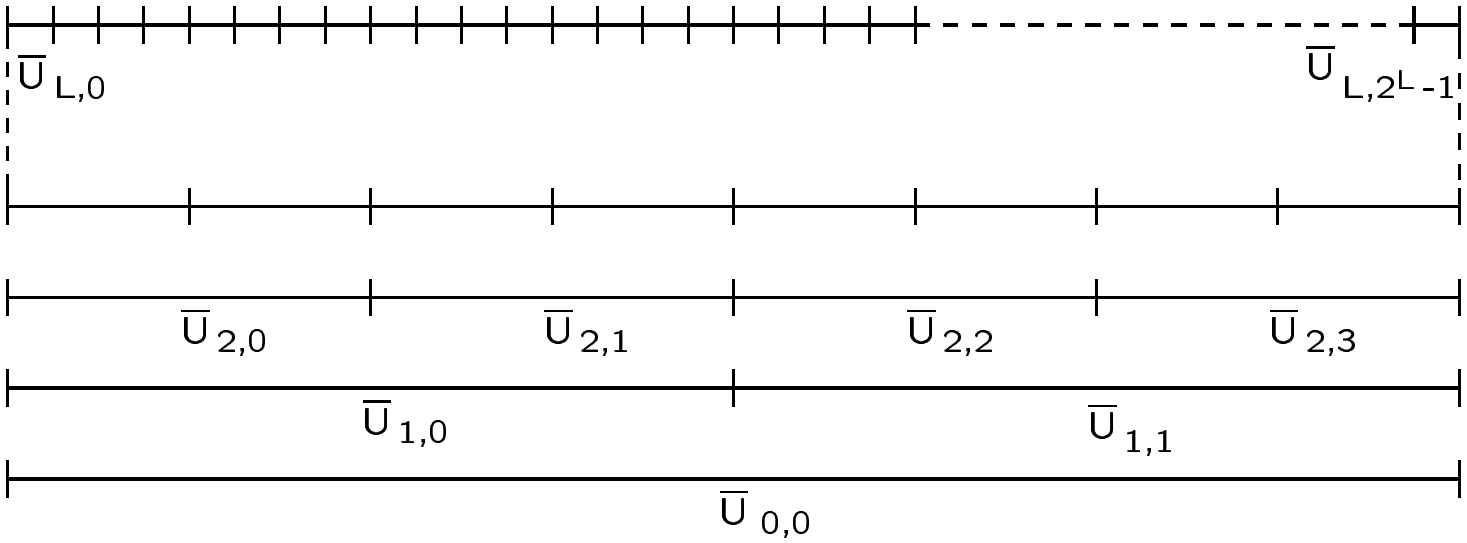

We denote by $\bar{U}_l = \left(U_{l,i}\right)_{0 \leq i < 2^l}$.

Harten multiresolution

Multiresolution decomposition for cell-average values

Projection : (or restriction) $\bar{U}_{l-1} = \mathbf{P}_{l \to l-1}\, \bar{U}_l$
Prediction : (or prolongation) $\hat{U}_{l+1} = \mathbf{P}_{l \to l+1}\, \bar{U}_l$

$\mathbf{P}_{l \to l+1}$ is **local** and **consistent with** $\mathbf{P}_{l \to l-1}$, i.e.

$$\mathbf{P}_{l \to l-1}\, \mathbf{P}_{l \to l+1} \;=\; \mathrm{Id}$$

Details: $D_{l,i} = \bar{U}_{l,i} - \hat{U}_{l,i}$. If $\mathbf{P}$ is consistent, they are redundant.

The knowledge of $\bar{U}$ for the N children is **equivalent** to the knowledge of $\bar{U}$ for the parent and $N-1$ details: $\bar{U}_l \leftrightarrow (\bar{U}_{l-1}, D_l)$.

Multiresolution transform : $\bar{\mathbf{M}} : \bar{U}_L \mapsto (\bar{U}_0, D_1, \ldots, D_L)$

Adaptive multiresolution method

Thresholding : Delete $D_{l,i}$ if $|D_{l,i}| < \epsilon_l \Rightarrow$ error controlled

Data : graded tree structure $\bar{U}_l = (\bar{u}_{l,i})_{0 \leq l \leq L,\, i \in \Lambda_l}$

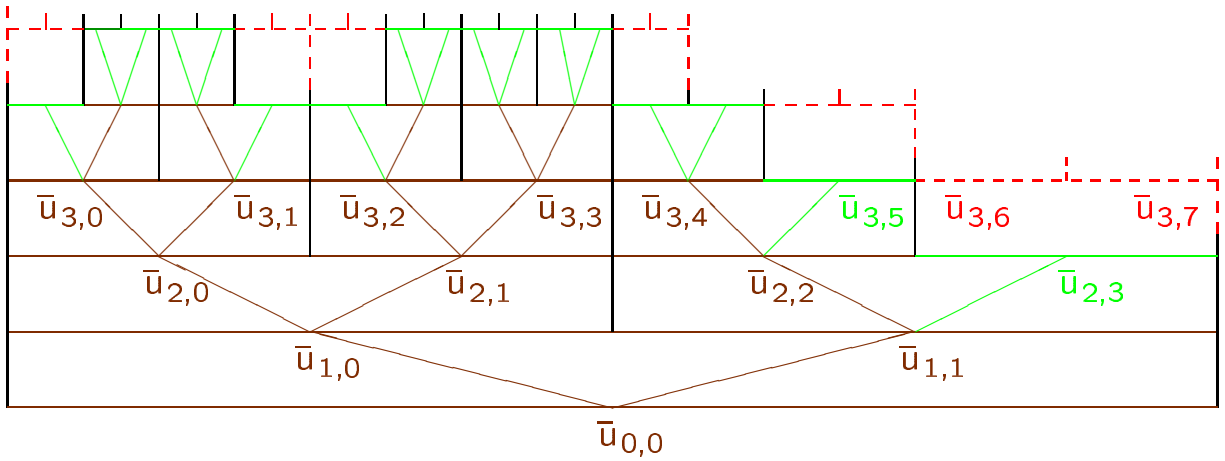

- nodes - leaves - virtual leaves

Adaptive multiresolution method

Discretization of the compressible Navier-Stokes equations

- **Compressible Navier-Stokes equations:** *non-linear parabolic equations of the form*

  $\partial_t U = \mathcal{D}(U)$, $U = (\rho, \rho\vec{v}, \rho e)^t$, and $\mathcal{D}(U) = -\nabla \cdot (f(U) + \phi(U, \nabla U)) + S(U)$

- **Explicit time and space discretization:**

  $$\forall (l,i) \in \Lambda,\ \partial_t \bar{U}_{l,i} = \bar{\mathcal{D}}_{l,i}$$

  with

  $$\bar{U}_{l,i} = \frac{1}{|\Omega_{l,i}|} \int_{\Omega_{l,i}} U \, d\mathcal{V}$$

  and

  $$\bar{\mathcal{D}}_{l,i} := \frac{1}{|\Omega_{l,i}|} \int_{\Omega_{l,i}} \mathcal{D} \, d\mathcal{V} = -\frac{1}{|\Omega_{l,i}|} \int_{\partial\Omega_{l,i}} (f(U) + \phi(U, \nabla U)) \cdot n_{l,i} \, ds + \bar{S}_i$$

Ref. Roussel, Schneider, Tsigulin, Bockhorn. JCP 188 (2003)

Adaptive multiresolution method

Algorithm

$$\bar{U}^{n+1} = \bar{\mathbf{M}}^{-1}\, \mathbf{T}(\epsilon)\, \bar{\mathbf{M}}\, \mathbf{E}(\Delta t)\, \bar{U}^{n}$$

- *Thresholding:* $\mathbf{T}(\epsilon)$
  - After thresholding, **one more level is added** $\Rightarrow$ undelete details
- *Time evolution*: $\mathbf{E}(\Delta t)$
  - Only on leaves. Virtual leaves are used for the *flux computation*.
  - To ensure **conservativity** : flux always computed on the *higher level*
- *Complexity*: $O(N \log N)$, $N =$ number of degrees of freedom

Ref. Roussel, Schneider, Tsigulin, Bockhorn. JCP 188 (2003)

Conservative flux computation

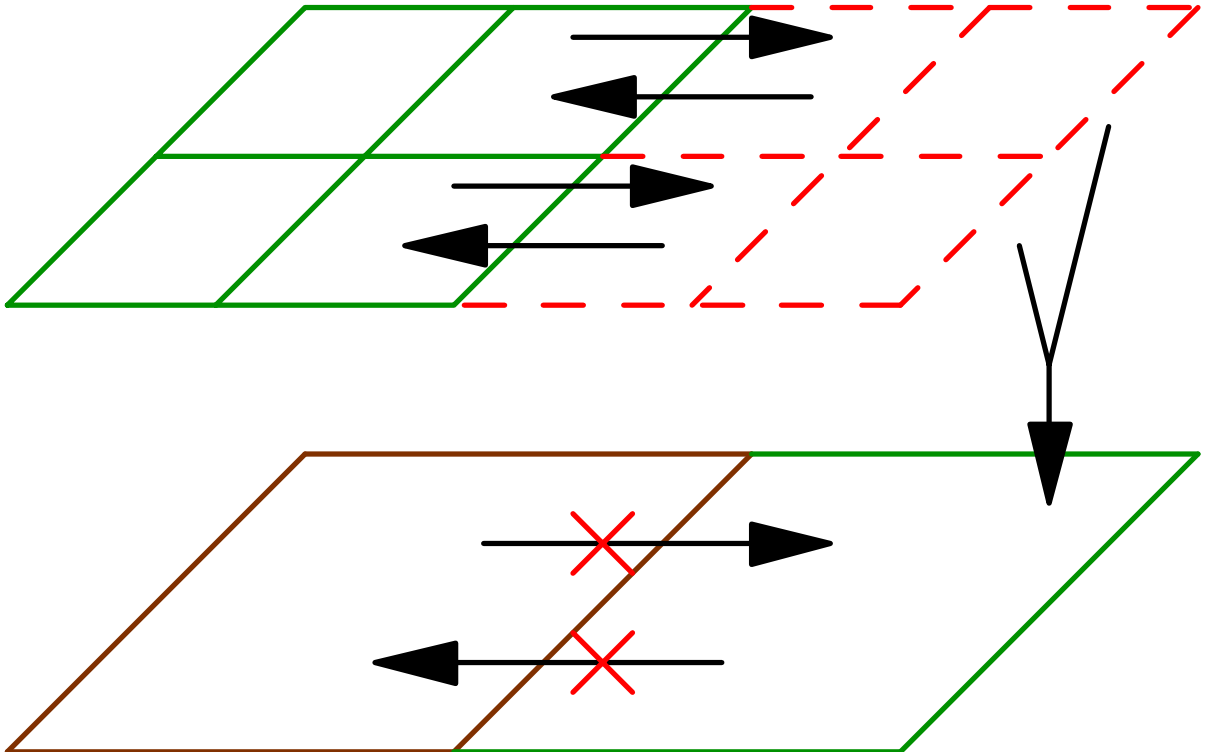

Ingoing and outgoing flux computation in 2D for two different levels

Ref. Roussel, Schneider, Tsigulin, Bockhorn. JCP 188 (2003)

Wavelet normalization

The detail $D_{l,i}$ is proportional to the wavelet coefficient $< U, \tilde{\psi}_{l,i} >$, $\tilde{\psi}_{l,i}$ being the **dual wavelet** function.

Biorthogonal wavelets $\rightarrow$ the choice of the wavelet basis is not unique.

$$| < U, \tilde{\psi}_{l,i} > | < \epsilon \Leftrightarrow |D_{l,i}| < \epsilon_l$$

- if $||\tilde{\psi}_{l,i}||_{L_1} = 1$, then $\epsilon_l = 2^{d(l-L)}\epsilon_L$.
- if $||\tilde{\psi}_{l,i}||_{L_2} = 1$, then $\epsilon_l = 2^{\frac{d}{2}(l-L)}\epsilon_L$.
- if $||\tilde{\psi}_{l,i}||_{H_1} = 1$, then $\epsilon_l = 2^{(\frac{d}{2}-1)(l-L)}\epsilon_L$.

All these normalizations will be tested.

Best normalization $\rightarrow$ for a given number of degrees of freedom, the one which contains the most coherent vortices.

Local Time Stepping (LTS) : main aspects

- On the finest scale L, Δt is imposed by the stability condition of the explicit scheme
- On larger scales $\ell < L$, $\Delta t^{\ell} = 2^{L-\ell}\Delta t$
- One LTS cycle: $t_n \longrightarrow t^{n+2^L}$
- At intermediate steps of the evolution of fine cells, required information of coarser neighbours are interpolated in time.

Scheme of local scale-dependent time-stepping

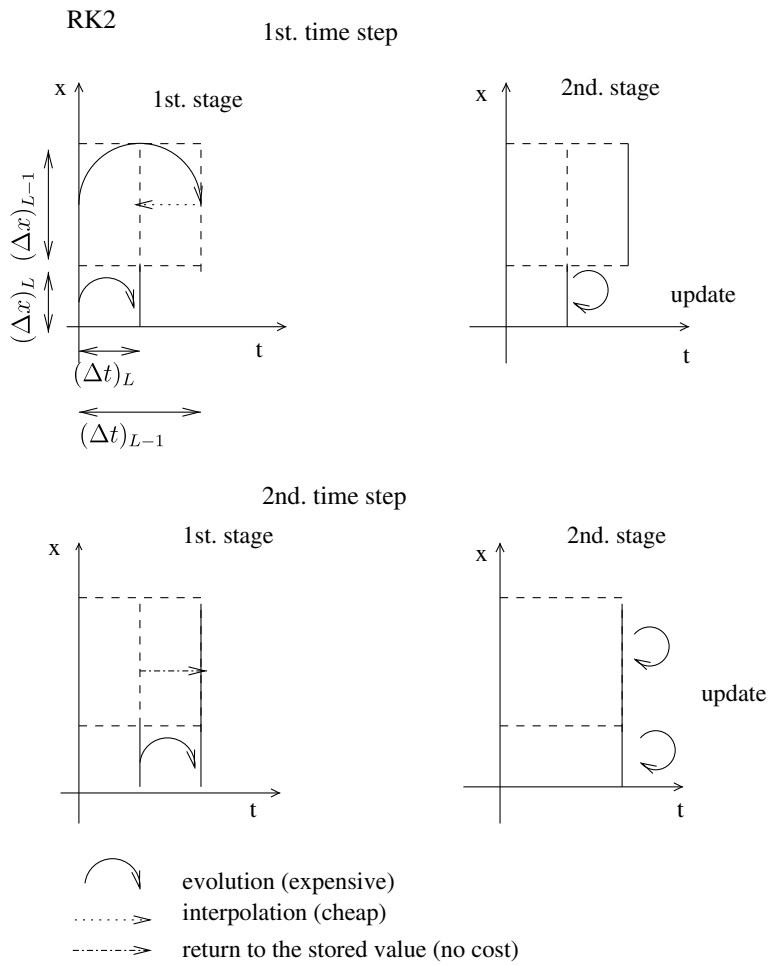

Ref. Domingues, Gomes, Roussel and Schneider. JCP 227 (2008)

Controlled Time Stepping (CTS) : main aspects

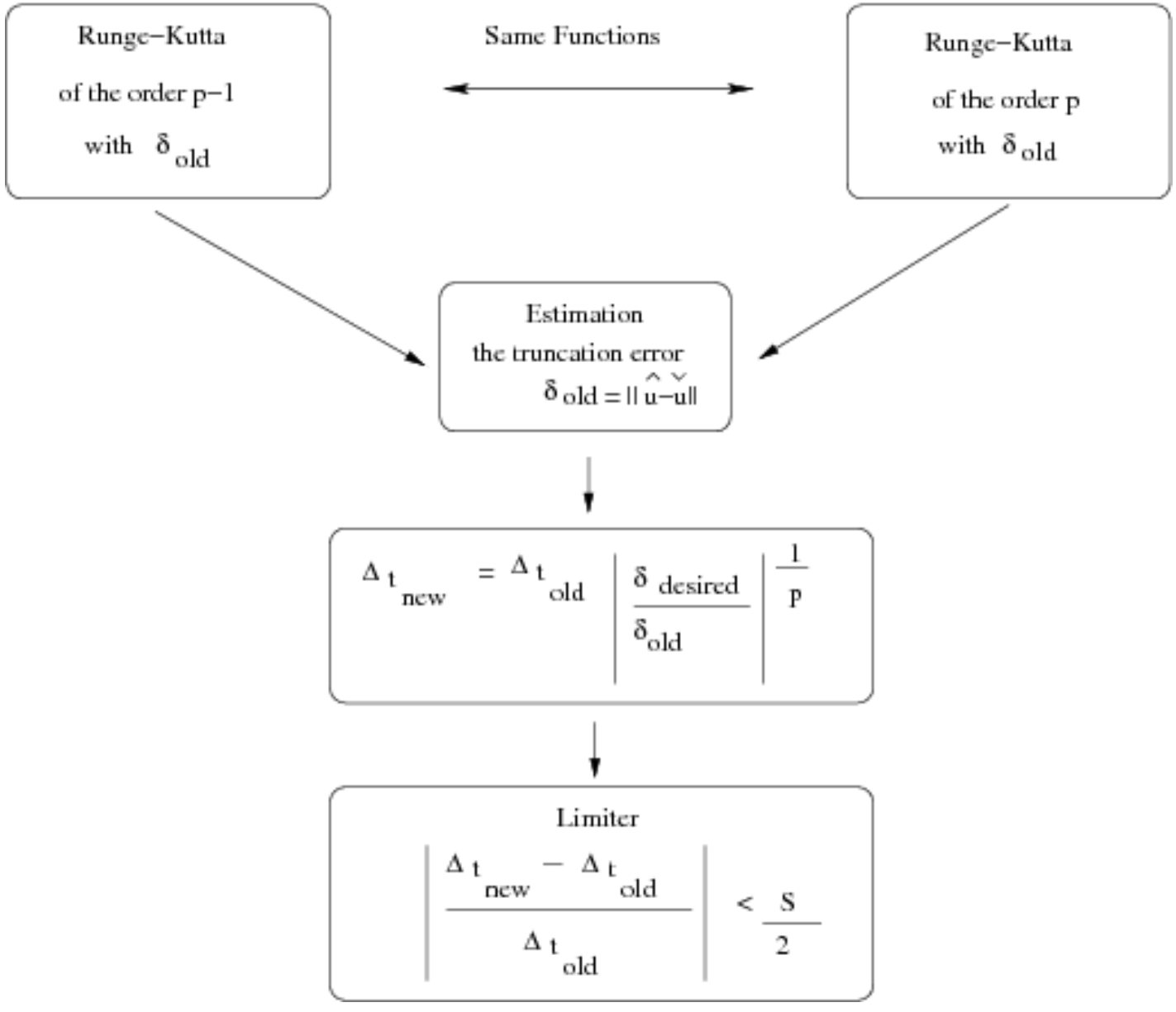

MR/CTS/LTS scheme

Combination of MR, CTS and LTS strategies:

1. MR/CTS is applied to determine the time step Δt required to attain a specified accuracy with a global time stepping;
2. the MR/LTS cycle is computed using the obtained step size Δt for the evolution of the cell averages on the finest scale;
3. another MR/CTS time step is then done to adjust the next time step, and so on.

Numerical validation

Error analysis

- *Stability*
  Convection-diffusion equation: $\partial_t u + \partial_x u = \frac{1}{Pe}\partial^2_{xx} u$, TVD if (Bihari 1996)

$$\Delta t \leq \frac{\Delta x^2}{4Pe^{-1} + \Delta x} \ , \ \Delta x \propto 2^{-L} \tag{7}$$

- *Accuracy*

$$||\bar{u}^L_{ex} - \bar{u}^L_{MR}|| \leq ||\bar{u}^L_{ex} - \bar{u}^L_{FV}|| + ||\bar{u}^L_{FV} - \bar{u}^L_{MR}|| \tag{8}$$

  Discretization error: $||\bar{u}^L_{ex} - \bar{u}^L_{FV}|| \propto 2^{-\alpha L}$
  Perturbation error: $||\bar{u}^L_{FV} - \bar{u}^L_{MR}|| \propto n\epsilon = \frac{T}{\Delta t}\epsilon$ (Cohen *et al* 2002)

  We want the perturbation error to be **of the same order** as the discretization error. Therefore we choose

$$\boxed{\epsilon = C\frac{2^{-(\alpha+1)L}}{Pe + 2^{L+2}} \ , \ C > 0} \tag{9}$$

Ref. Roussel, Schneider, Tsigulin, Bockhorn. JCP 188 (2003)

Numerical validation

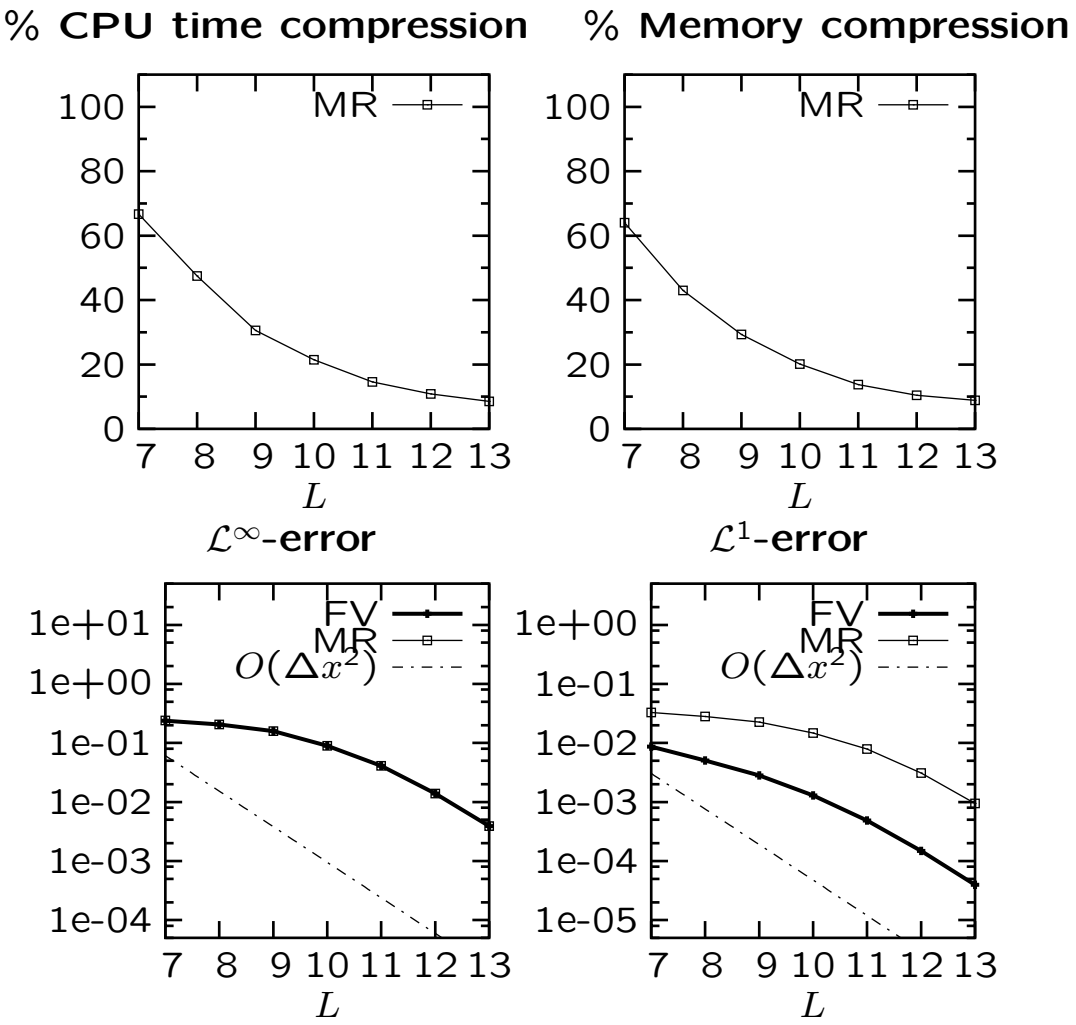

Convection-diffusion: $Pe = 10000$, $t = 0.2$, $C = 5.10^8$

Numerical validation

Viscous Burgers equation: $\partial_t u + \partial_x \left(\frac{u^2}{2}\right) = \frac{1}{Re}\partial^2_{xx} u$
Analogously, we set

$$\epsilon = C\frac{2^{-(\alpha+1)L}}{Re + 2^{L+2}} \ , \ C > 0 \qquad (10)$$

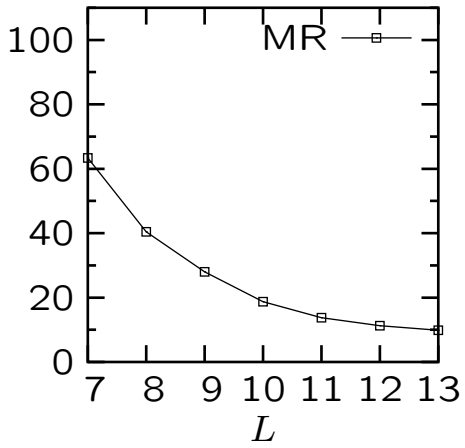

% CPU time compression

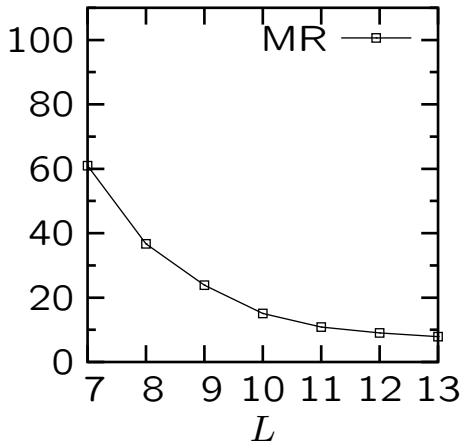

% Memory compression

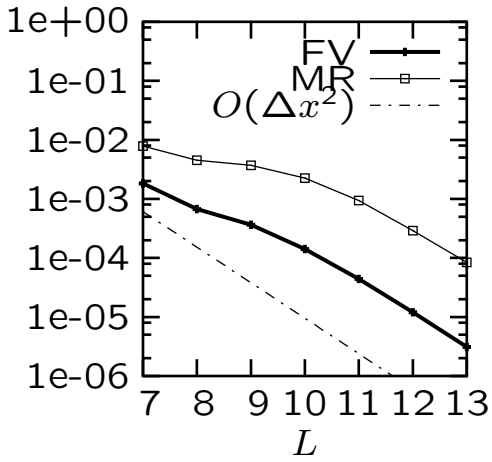

$\mathcal{L}^1$-error

$Re = 1000$, $t = 0.2$, $C = 5.10^8$

Ref. Roussel, Schneider, Tsigulin, Bockhorn. JCP 188 (2003)

Coherent Vortex Simulation

Compressible Navier-Stokes equations

Turbulent weakly compressible 3d mixing layer

Coherent Vortex Simulation

total = coherent + incoherent

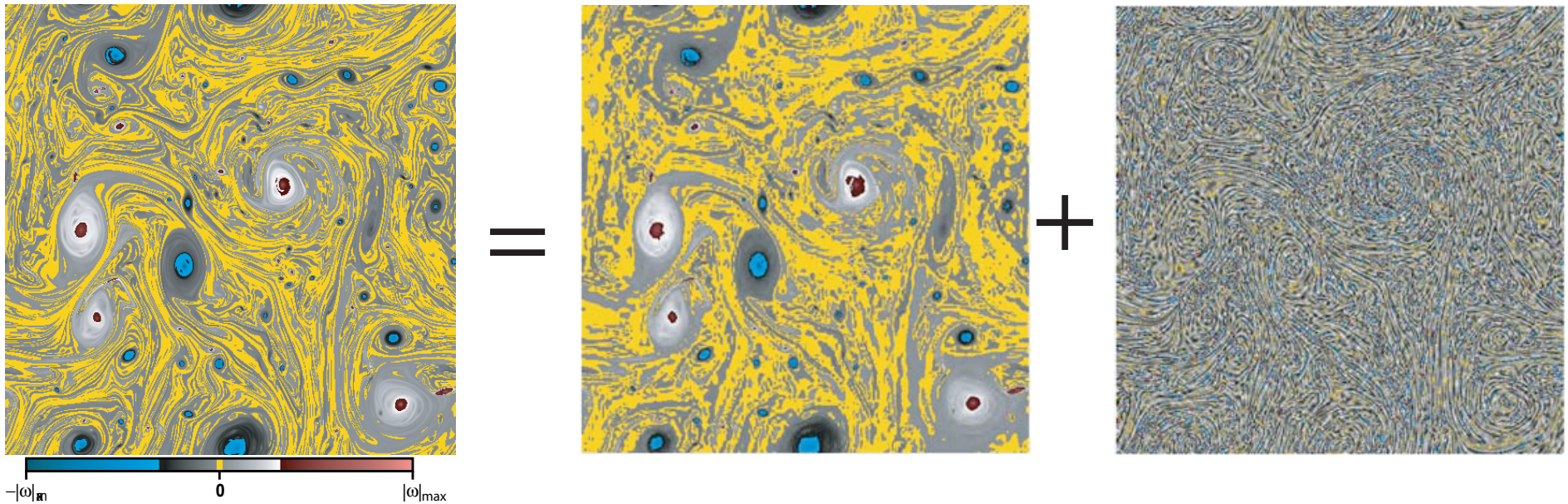

2d vorticity field

(M. Farge and K. Schneider. *Flow, Turbulence and Combustion*, 66, 2001.).

see also K. Schneider and O. Vasilyev. Wavelet methods in CFD. Annu. Rev. Fluid Mech., 42, 2010.

Principle of CVS (I)

CVS of incompressible turbulent flows: decomposition of the vorticity $\omega = \nabla \times u$ into coherent and incoherent parts using thresholding of the wavelet coefficients.

Evolution of the coherent flow is then computed deterministically in a dynamically adapted wavelet basis and the influence of the incoherent components is statistically modelled (Farge & Schneider 2001).

Here: compressible flows.

Decompose the conservative variables $U = (\rho,\ \rho u_1,\ \rho u_2,\ \rho u_3,\ \rho e)$ into a biorthogonal wavelet series.

A decomposition of the conservative variables into coherent and incoherent components is then obtained by decomposing the conservative variables into wavelet coefficients, applying a thresholding and reconstructing the coherent and incoherent contributions from the strong and weak coefficients, respectively.

Principle of CVS (II)

Dimensionless density and pressure are decomposed into

$$\begin{aligned} \rho &= \rho_C + \rho_I \,, \\ p &= p_C + p_I \,. \end{aligned} \tag{5}$$

where ρ_C and p_C respectively denote the coherent part of the density and pressure fields, while ρ_I and p_I denote the corresponding incoherent parts.

Velocity u_1, u_2, u_3, temperature T and energy e, are decomposed using the Favre averaging technique, i.e. density weighted.

For a quantity φ we obtain,

$$\varphi = \varphi_C + \varphi_I \;, \text{ where } \varphi_C = \frac{(\rho\varphi)_C}{(\rho)_C} \tag{6}$$

Finally, retaining only the coherent contributions of the conservative variables we obtain the filtered compressible Navier-Stokes equations which describe the flow evolution of the coherent flow U_C. The influence of the incoherent contributions U_I is in the current approach completely negleted.

Navier–Stokes equations for compressible flows (I)

Three-dimensional compressible flow of a Newtonian fluid in the Stokes hypothesis in a domain $\Omega \subset \mathbb{R}^3$.

$$
\begin{aligned}
\frac{\partial \rho}{\partial t} &= -\frac{\partial}{\partial x_j}\left(\rho\, u_j\right) \\
\frac{\partial}{\partial t}\left(\rho\, u_i\right) &= -\frac{\partial}{\partial x_j}\left(\rho\, u_i\, u_j + p\, \delta_{i,j} - \tau_{i,j}\right) \\
\frac{\partial}{\partial t}\left(\rho\, e\right) &= -\frac{\partial}{\partial x_j}\left(\left(\rho\, e + p\right)\, u_j - u_i\, \tau_{i,j} - \lambda \frac{\partial T}{\partial x_j}\right)
\end{aligned}
$$

ρ, p,T and e denote the dimensionless density, pressure, temperature and specific total energy per unit of mass, respectively; $(u_1, u_2, u_3)^T$ is the dimensionless velocity vector.

Navier–Stokes equations for compressible flows (II)

The components of the dimensionless viscous strain tensor $\tau_{i,j}$ are

$$\tau_{i,j} = \frac{\mu}{Re}\left(\frac{\partial u_i}{\partial x_j} + \frac{\partial u_j}{\partial x_i} - \frac{2}{3}\frac{\partial u_k}{\partial x_k}\,\delta_{i,j}\right) ,$$

where μ denotes the dimensionless molecular viscosity and Re the Reynolds number. The dimensionless conductivity λ is defined by

$$\lambda = \frac{\mu}{(\gamma - 1)\; Ma^2\; Re\; Pr} ,$$

where γ, Ma and Pr respectively denote the specific heat ratio and the Mach and Prandtl numbers.

The system is completed by an equation of state for a calorically ideal gas

$$p = \frac{\rho\, T}{\gamma\; Ma^2} .$$

and suitable initial and boundary conditions.

Navier–Stokes equations for compressible flows (III)

Assuming the temperature to be larger than 120 K, the molecular viscosity varies with the temperature according to the dimensionless Sutherland law

$$\mu = T^{\frac{3}{2}} \left(\frac{1 + T_s}{T + T_s} \right)$$

where $T_s \approx 0.404$.

Denoting by (x, y, z) the three Cartesian directions, this system of equations can be written in the following compact form

$$\frac{\partial U}{\partial t} = -\frac{\partial F}{\partial x} - \frac{\partial G}{\partial y} - \frac{\partial H}{\partial z}$$

where $U = (\rho,\ \rho u_1,\ \rho u_2,\ \rho u_3,\ \rho e)^T$ denotes the vector of the conservative quantities, and F, G, H are the flux vectors in the directions x, y, and z, respectively.

Time evolution (I)

Explicit 2-4 Mac Cormack scheme, which is second-order accurate in time, fourth-order in space for the convective terms, and second-order in space for the diffusive terms

$$\begin{aligned}
\bar{U}^{*}_{l,i,j,k} = \bar{U}^{n}_{l,i,j,k} \quad &+ \quad \Delta t \left(\frac{-7\ \bar{F}^{n}_{l,i,j,k} + 8\ \bar{F}^{n}_{l,i+1,j,k} - \bar{F}^{n}_{l,i+2,j,k}}{6\Delta x} \right) \\
&+ \quad \Delta t \left(\frac{-7\ \bar{G}^{n}_{l,i,j,k} + 8\ \bar{G}^{n}_{l,1,j+1,k} - \bar{G}^{n}_{l,i,j+2,k}}{6\Delta y} \right) \\
&+ \quad \Delta t \left(\frac{-7\ \bar{H}^{n}_{l,i,j,k} + 8\ \bar{H}^{n}_{l,1,j,k+1} - \bar{H}^{n}_{l,i,j,k+2}}{6\Delta z} \right)
\end{aligned}$$

Time evolution (II)

$$\bar{U}^{n+1}_{l,i,j,k} = \frac{\bar{U}^{n}_{l,i,j,k} + \bar{U}^{*}_{l,i,j,k}}{2} + \frac{\Delta t}{2}\left(\frac{-7\ \bar{F}^{n}_{l,i,j,k} + 8\ \bar{F}^{n}_{l,i-1,j,k} - \bar{F}^{n}_{l,i-2,j,k}}{6\Delta x}\right) + \frac{\Delta t}{2}\left(\frac{-7\ \bar{G}^{n}_{l,i,j,k} + 8\ \bar{G}^{n}_{l,1,j-1,k} - \bar{G}^{n}_{l,i,j-2,k}}{6\Delta y}\right) + \frac{\Delta t}{2}\left(\frac{-7\ \bar{H}^{n}_{l,i,j,k} + 8\ \bar{H}^{n}_{l,1,j,k-1} - \bar{H}^{n}_{l,i,j,k-2}}{6\Delta z}\right)$$

Note that, for the computation of the diffusive terms, we do not use a decentered scheme. Here the diffusive terms are approximated the same way as if we were using a second-order Runge-Kutta-Heun method in time, together with a second-order centered scheme in space.

Coherent Vortex Simulation

- **Test-case**: 3D compressible, temporally developing mixing layer
- Computational domain $\Omega = [-30, 30]^3$
- $Ma = 0.3$, $Pr = 0.7$, no forcing
- Reynolds based on half vorticity thickness $Re = 50$
- Dimensionless physical time $t = 80$
- Maximal resolution $N = 128^3$
- Initial perturbation $\rightarrow$ quasi two-dimensional
- Comparison with DNS using the same numerical schemes
- **No statistical model used**: incoherent part is only discarded.

Flow configuration of the mixing layer

We initialize the test-case by setting two layers of a fluid stacked one upon the other one, each of them with the same velocity norm but opposed directions.

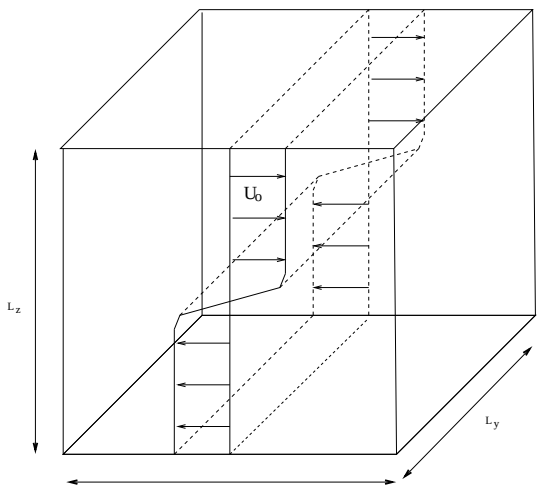

Fig. 2. Flow configuration: domain and initial basic flow $\boldsymbol{u}_0$ of the three-dimensional mixing layer.

Coherent Vortex Simulation

Top : isolines of vorticity 0.5 (red) and 0.25 (yellow). Bottom : slice at $y = 0$.

Coherent Vortex Simulation

Slices of vorticity at y = 0

Coherent Vortex Simulation

Adaptive grid

Coherent Vortex Simulation

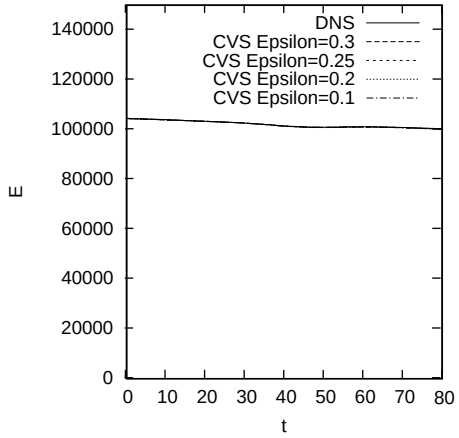

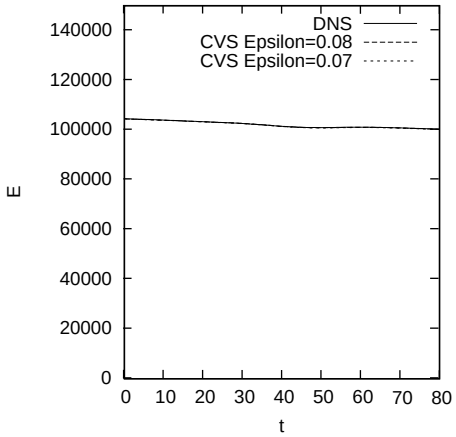

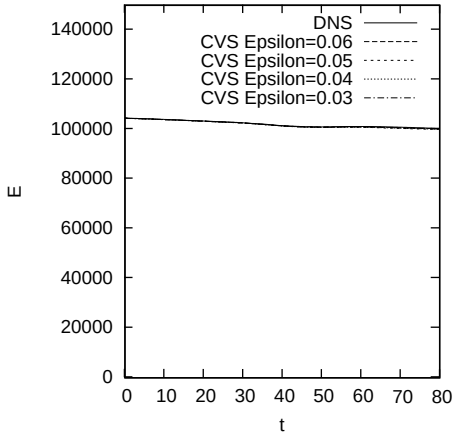

Time evolution of the kinetic energy: norm L_1 (left), norm L_2 (center), norm H_1 (right)

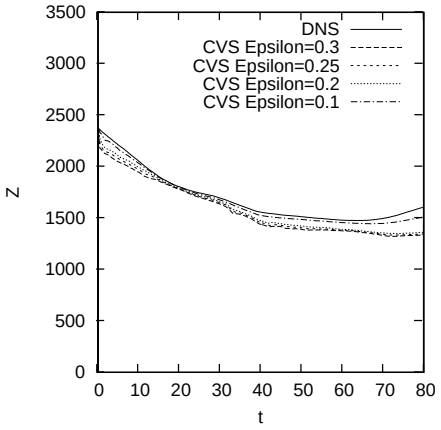

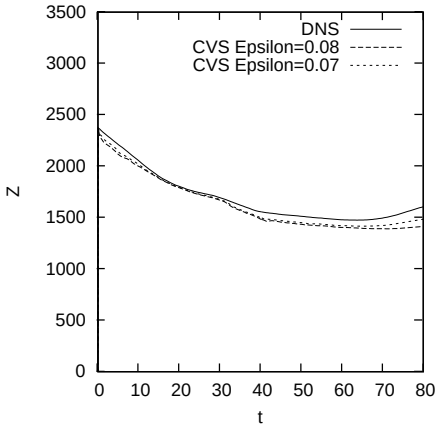

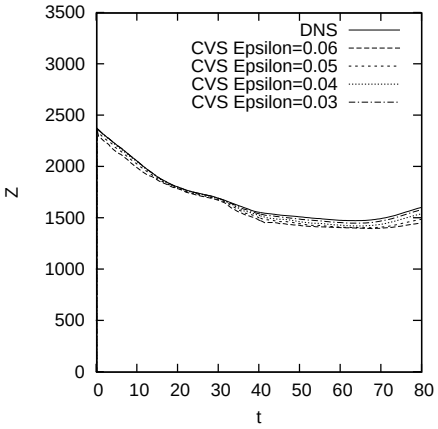

Time evolution of the enstrophy: norm L_1 (left), norm L_2 (center), norm H_1 (right)

Coherent Vortex Simulation

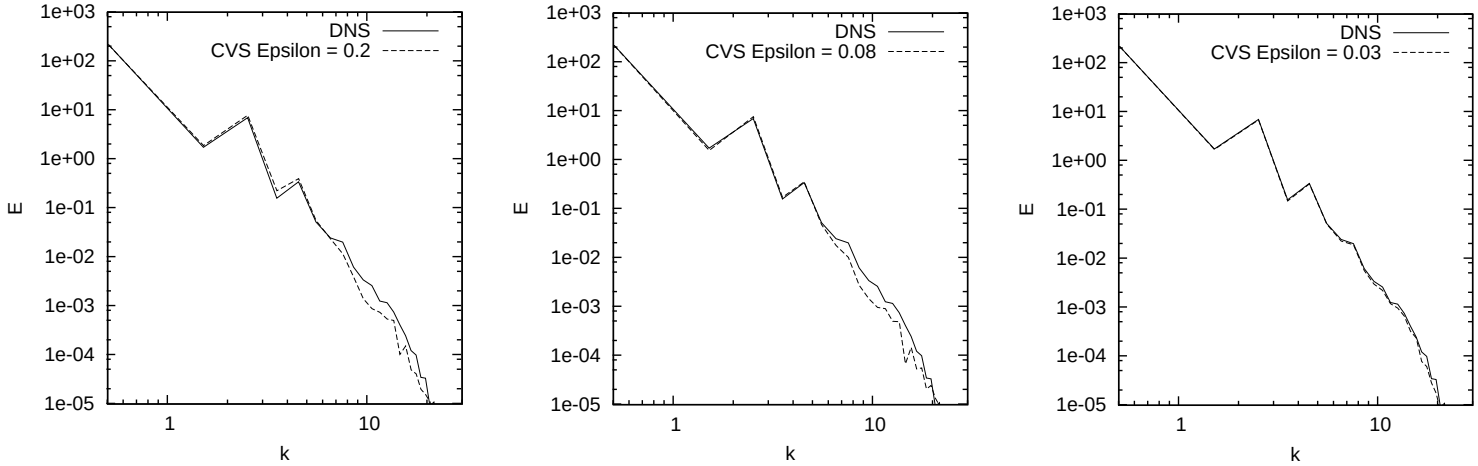

Energy spectrum at $t = 80$: norm L_1 (left), norm L_2 (center), norm H_1 (right)

Method	*Norm*	ε	*CPU time*	*% CPU*	*% Mem*	*% E*	*% Z*
DNS			7d 6h	100 %	100 %	100 % %	100 %
CVS	L_1	0.2	2d 13h	35.05 %	33.44 %	99.92 %	84.85 %
CVS	L_2	0.08	2d 18h	37.93 %	30.55 %	99.96 %	88.17 %
CVS	H_1	**0.03**	**2d 8h**	**32.18 %**	**34.54 %**	**99.88 %**	**98.66 %**

Coherent Vortex Simulation

- **Test-case**: 3D compressible, temporally developing mixing layer
- Computational domain $\Omega = [-60, 60]^3$
- $Ma = 0.3$, $Pr = 0.7$, no forcing
- Reynolds based on half vorticity thickness $Re = 200$
- Dimensionless physical time $t = 80$
- Maximal resolution $N = 256^3$, pictures downsampled on 128^3
- Initial perturbation $\longrightarrow$ quasi two-dimensional
- **No statistical model used**: incoherent part is only discarded.
- CPU time compression **23.12 %**, memory compression **16.86 %**

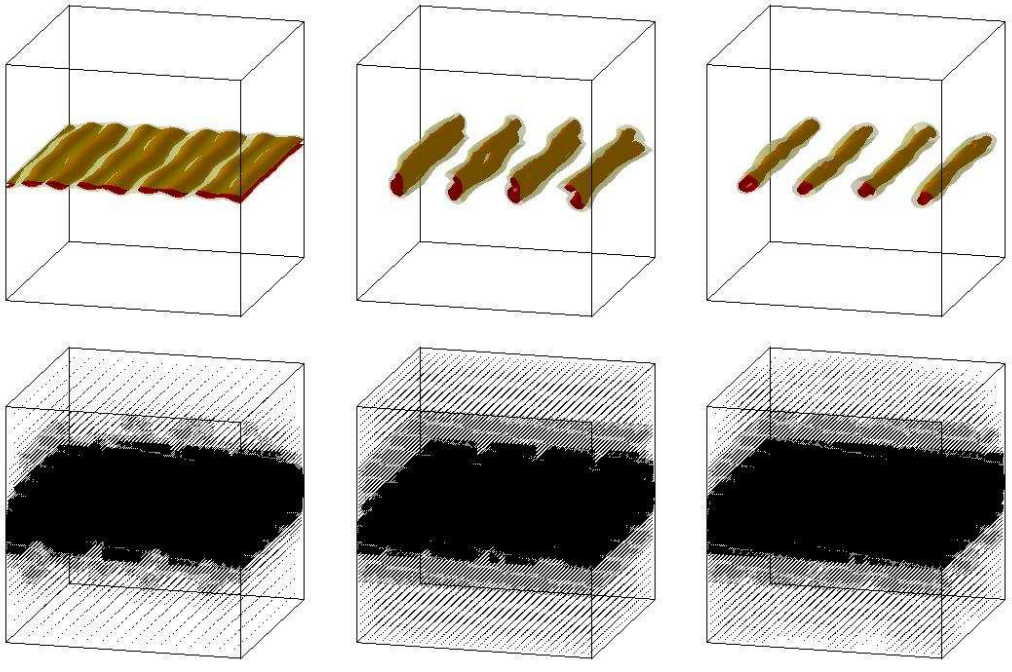

Fig. 17. Time evolution of a weakly compressible mixing layer at resolution $N = 256^3$ in the quasi-2D regime. CVS computation with $\epsilon = 0.03$ and norm #3. First row: Two-dimensional cut of vorticity at $y = 0$, 10 isolines of vorticity between 0.1 and 1. Second row: Corresponding isosurfaces of vorticity $||\omega|| = 0.5$ *(black)* and $||\omega|| = 0.25$ *(gray)*. Third Row: Corresponding adaptive mesh of the CVS computation. The corresponding time instants are t = 19 *(left)*, t = 37 *(center)* and t = 78 *(right)*.

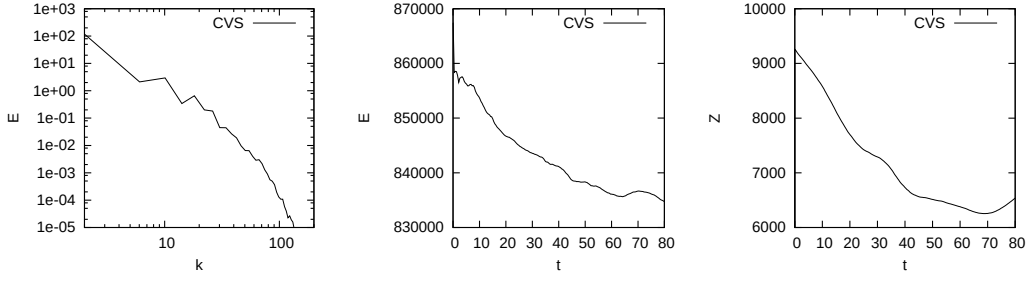

Fig. 18. Energy spectra in the streamwise direction at $t = 80$ *(left)*. Time evolution of the kinetic energy *(center)* and enstrophy *(right)* for the CVS computations at $Re = 200$, $N = 256^3$.

Conclusions (CVS I)

Adaptive multiresolution method to solve the three-dimensional compressible Navier–Stokes equations in a Cartesian geometry.

Extension of the Coherent Vortex Simulation approach to compressible flows.

Time evolution of the coherent flow contributions computed efficiently using the adaptive multiresolution method.

Generic test case: weakly compressible turbulent mixing layers.

Different thresholding rules, i.e. L^1, L^2 and H^1 norms.

H^1 based threshold yields the best results in terms of accuracy and efficiency.

Conclusions (CVS II)

CVS required only about 1/3 of the CPU time needed for DNS and allows furthermore a memory reduction by almost a factor 5. Nevertheless all dynamically active scales of the flow are well resolved.

Drawbacks:

Explicit time discretization, imposes a time step limitation due to stability reasons, i.e. the smallest spatial scale dictates the actual size of the time step ($\longrightarrow$ local time stepping strategies).

Using local time stepping the time step on larger scales can be increased without violating the stability criterion of the explicit time integration (further speed up).

Generalisation to complex geometries: volume penalization approach (cf. Angot et al. 1999, Schneider & Farge 2005).

Compressible Euler equations

Multiresolution or Adaptive Mesh Refinement ?

2D Riemann problem: Lax-Liou test case 5

3D expanding circular shock wave

R.Deiterding, M.Domingues, S.Gomes, O.Roussel and K.Schneider. ESAIM Proc., 2009, to appear.

2D/3D Euler equations

The compressible Euler equations:

$$\frac{\partial Q}{\partial t}+\frac{\partial F}{\partial \vec{r}}=0, \quad \text{with} \quad Q=\begin{pmatrix} \rho \\ \rho\vec{v} \\ \rho e \end{pmatrix} \quad \text{and} \quad F=\begin{pmatrix} \rho\vec{v} \\ \rho u^2+p \\ (\rho e+p)\vec{v} \end{pmatrix}$$

where t is time,
$\vec{r}$ is 2D position vector with $|\vec{r}|=\sqrt{(x^2+y^2)}$,
$\rho=\rho(\vec{r},t)$ density,
$\vec{v}=\vec{v}(\vec{r},t)$ velocity with components (v_1,v_2),
$e=e(\vec{r},t)$ energy per unit of mass and
$p=p(\vec{r},t)$ pressure.

The equation of state for an ideal gas

$$p = \rho R T = (\gamma - 1)\,\rho \left(e - \frac{|\vec{v}|^2}{2} \right),$$

completes the system, where
$T = T(\vec{r}, t)$ is temperature,
γ specific heat ratio and
R universal gas constant.

In dimensionless form, we obtain the same system of equations, but the equation of state becomes $p = \frac{\rho T}{\gamma Ma^2}$, where Ma denotes the Mach number.

Inviscid implosion phenomenon (2d)

The initial conditions are

$$\rho(r,0) = \begin{cases} 1 & \text{if} \quad r \leq r_0 \\ 0.125 & \text{if} \quad r > r_0, \end{cases}$$

$$\rho e(r,0) = \begin{cases} 2.5 & \text{if} \quad r \leq r_0 \\ 0.25 & \text{if} \quad r > r_0, \end{cases}$$

$v_1 = v_2 = 0$ and r_0 denotes the initial radius.
This initial condition is stretched in one direction and a rotation in the axes is applied.

$$r = \sqrt{\frac{X^2}{a^2} + \frac{Y^2}{b^2}},$$

$$\begin{aligned} X &= x\cos\theta - y\sin\theta, \\ Y &= -x\sin\theta + y\cos\theta \end{aligned}$$

The parameters of the ellipse: $a = 1/3$, $b = 1$, the rotation angle is $\theta = -\pi/3$ with an initial radius $r_0 = 1$, computational domain is $\Omega = [-2,2]^2$,$\epsilon = 10^{-2}$.

Ref.: Domingues et al., ANM, 59, 2009.

Multiresolution Computation : elliptical implosion

Density

Grid

Ref.: Domingues et al., ANM, 59, 2009.

Comparison for the numerical solutions of the 2D Euler equations for $t = 0.5$ with $L = 10$ and $\epsilon = 2 \cdot 10^{-3}$.

Method	Error	CPU		
	E	Time		Memory
	(%)	(10^3 sec)	(%)	(%)
FV-RK2, **CFL(0)=0.18** (Ref.)	0.60	45	100	100
MR-RK2, $CFL(0) = 0.18$	0.67	10	23	18
MR/LTS-RK2, $CFL(0) = 0.18$	1.09	9	19	16
MR/CTS/LTS-RK2(3), $CFL(0) = 0.24$	0.66	8	18	18
FV-RK3, **CFL(0)=0.18** (Ref.)	0.59	65	100	100
MR-RK3, $CFL(0) = 0.18$	0.66	12	18	18
MR/CTS-RK2(3), $CFL(0) = 0.24$	0.63	9	14	18

2d Riemann problem: Lax-Liu test case 5

Computational domain is $\Omega = [0,1] \times [0,1]$,
4 free-slip boundary conditions and
Physical parameters $Ma = 1$ and $\gamma = 1.4$.

Initial conditions:

Parameters	Domain position			
	1	2	3	4
Density(ρ)	1.00	2.00	1.00	3.00
Presure (p)	1.00	1.00	1.00	1.00
Velocity Component (v_1)	-0.75	-0.75	0.75	0.75
Velocity Component (v_2)	-0.50	0.50	0.50	-0.50

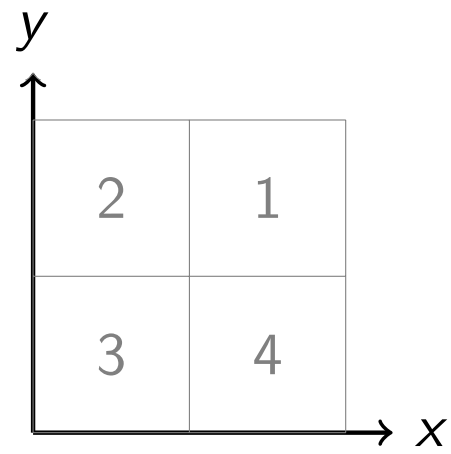

MR and AMR computations

MR method: 2nd order MUSCL with AUSM+-up Scheme flux vector splitting Liou(JCP, 2006) with van Albada limiter is used. RK2. Wavelet threshold $\epsilon = 0.01$.

AMR method: 2nd order unsplit shock-capturing MUSCL scheme with AUSMDV flux vector splitting Wada& Liou (SIAM J.Comput. Sci., 1997) . Limiting and reconstruction in primitive variables with Minmod limiter. Modified RK2. Adaptive parameters $\eta_\rho = \eta_{\boldsymbol{p}} = 0.05$ and $\epsilon_{\boldsymbol{p}} = \epsilon_\rho = 0.05$, with coarser level 128×128.

Computations at final time 0.3.
Target CFL number is 0.45.

In collaboration with Ralf Deiterding, Oak Ridge, USA

Adaptive Multiresolution Computation : Lax-Liu test case 5

Density

Grid

AMR simulation

Uniform
$\Delta x = 1/1024$

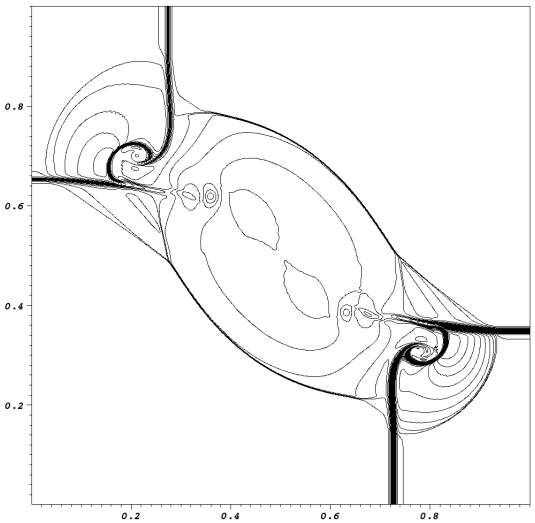

$r_{1,2,3} = 2, 2, 2$
$\Delta x = 1/1024$

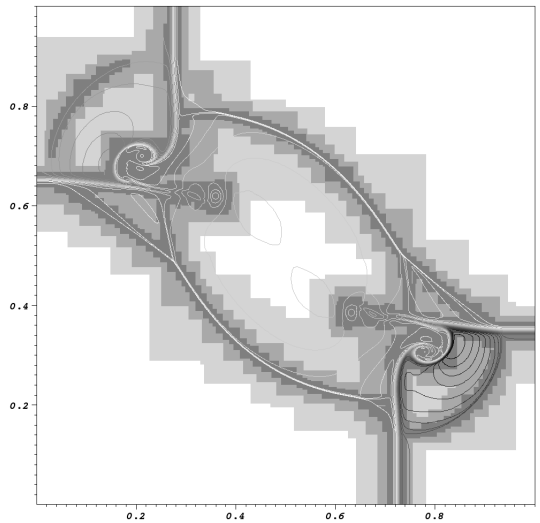

Reference solution
$x = 1/4096$

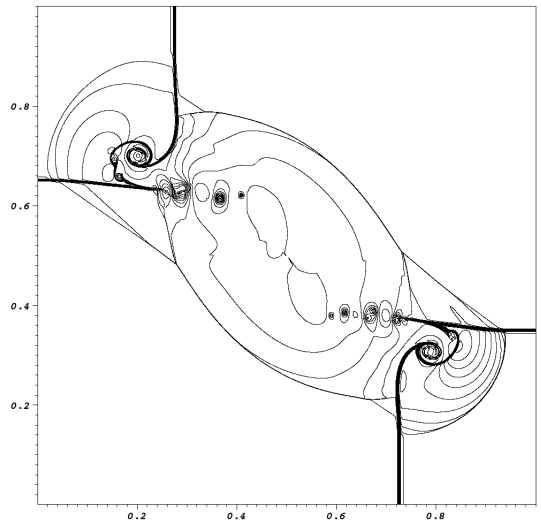

Reference solution computed with Wave Propagation Method.

In collaboration with Ralf Deiterding, Oak Ridge, USA

Summary of the results for MR and AMR/LT

Level	MR			
	$L_1^e(\rho)$ $[10^{-2}]$	Overhead per it. cell	Grid Compression (%)	Overhead per it. (%)
L=8	4.13	0.58	24.98	14.6
L=9	2.79	0.52	13.23	6.8
L=10	1.84	0.63	6.58	4.2

Level	AMR			
	$L_1^e(\rho)$ $[10^{-2}]$	Overhead per it. cell	Grid Compression (%)	Overhead per it. (%)
L=8	4.00	0.13	68.2	8.7
L=9	2.66	0.03	44.4	1.3
L=10	1.57	0.12	26.2	3.1

In collaboration with Ralf Deiterding, Oak Ridge, USA

Preliminary results

3d expanding circular shock-wave

As 3D test case, we study an inviscid expansion phenomenon in a square periodic box which contains the same gas, but with different conditions of pressure and temperature.
The initial condition is given by

$$Q(\vec{r}, t=0) = \begin{cases} \begin{pmatrix} 5 \\ \vec{0} \\ 12.5 \end{pmatrix} & \text{for } |\vec{r}| < r_0, \\ \begin{pmatrix} 1 \\ \vec{0} \\ 2.5 \end{pmatrix} & \text{otherwise.} \end{cases}$$

The computational domain is $\Omega = [0,1] \times [0,1] \times [0,1]$.
The computations are performed until $t = 0.84$.
The physical parameters are $Ma = 1$ and $\gamma = 1.4$.

MR computations

Numerical Parameters: $L = 7$, $\epsilon = 0.001$, RK2 scheme, MUSCL AUSM+up flux, $CFL = 0.8$.

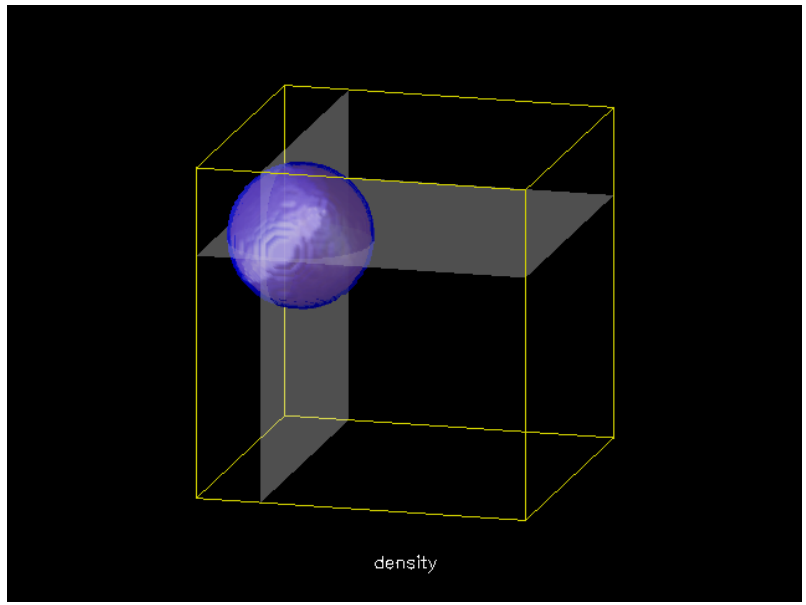

Density initial condition.

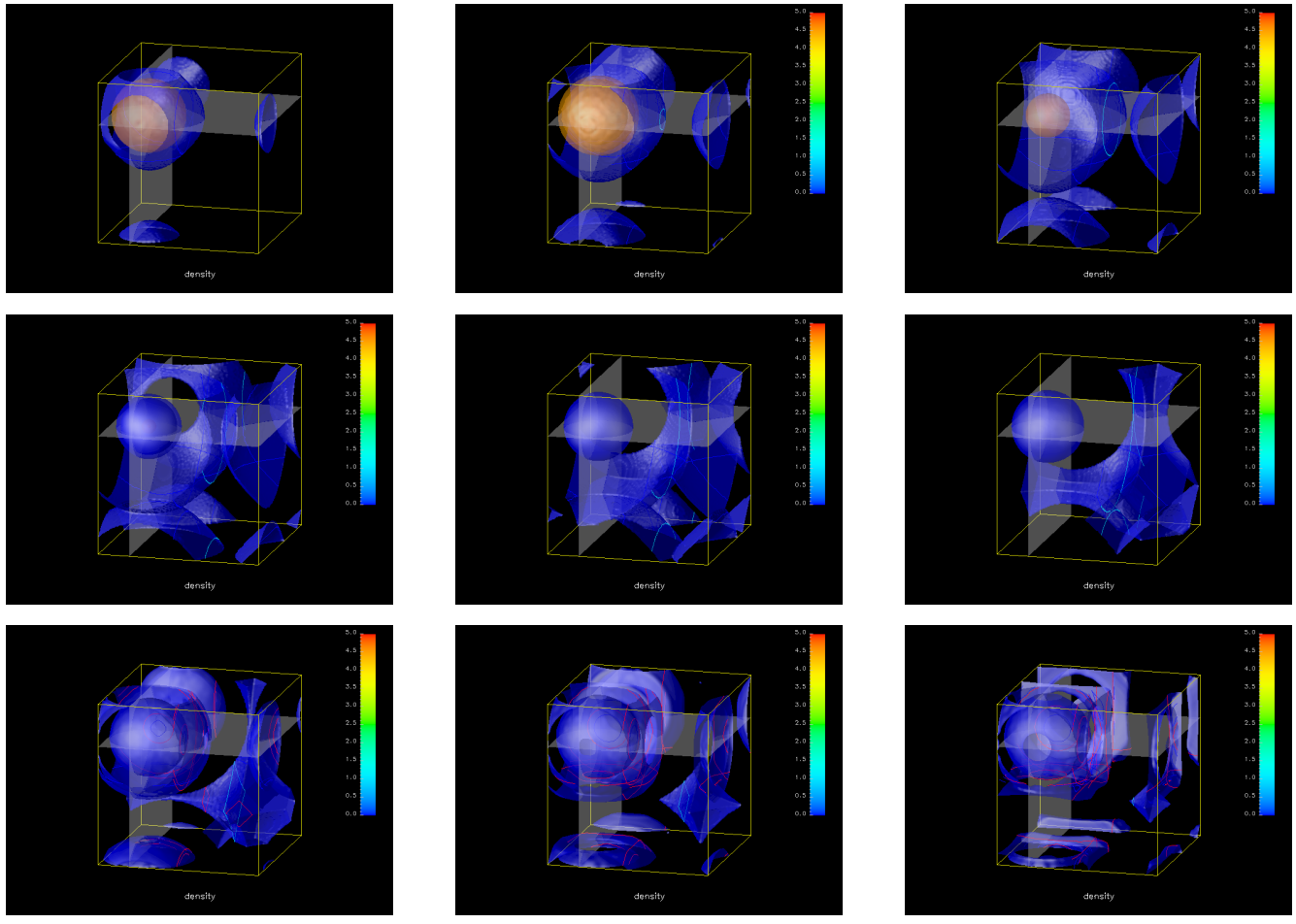

Evolution of density at
$t = 0.042, 0.084, 0.126, 0.210, 0.252, 0.294, 0.336, 0.378, 0.420$
(from left to right and top to bottom).

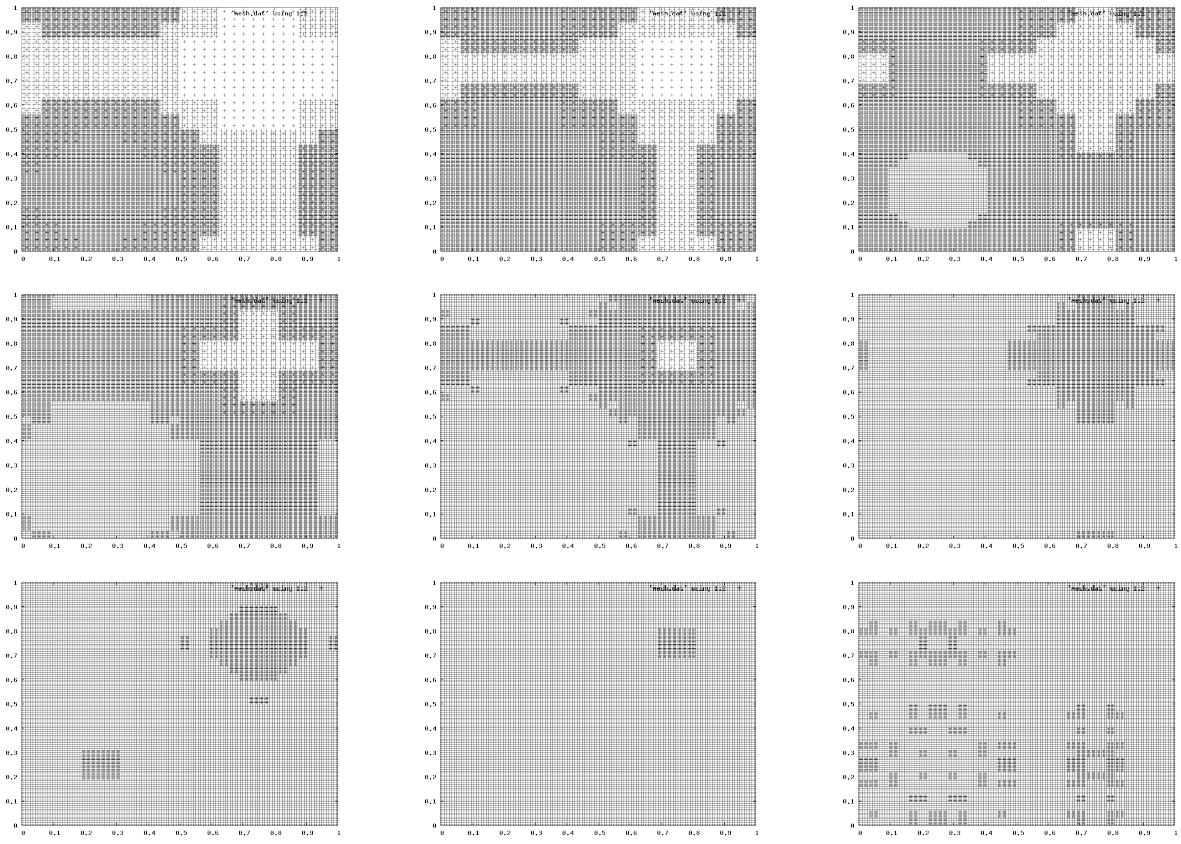

Adaptive grid: xy projection grid at
$t = 0.042, 0.084, 0.126, 0.210, 0.252, 0.294, 0.336, 0.378, 0.420$
(from left to right and top to bottom).

AMR computations

Numerical Parameters: 2 levels with refinement factor 2 are used, finest level: $120 \times 120 \times 120$ grid (1.73 M cells), coarse grid of $30 \times 30 \times 30$ cells, minmod-limiter, $CFL = 0.8$, until physical time $t = 0.84$, 58 time steps.

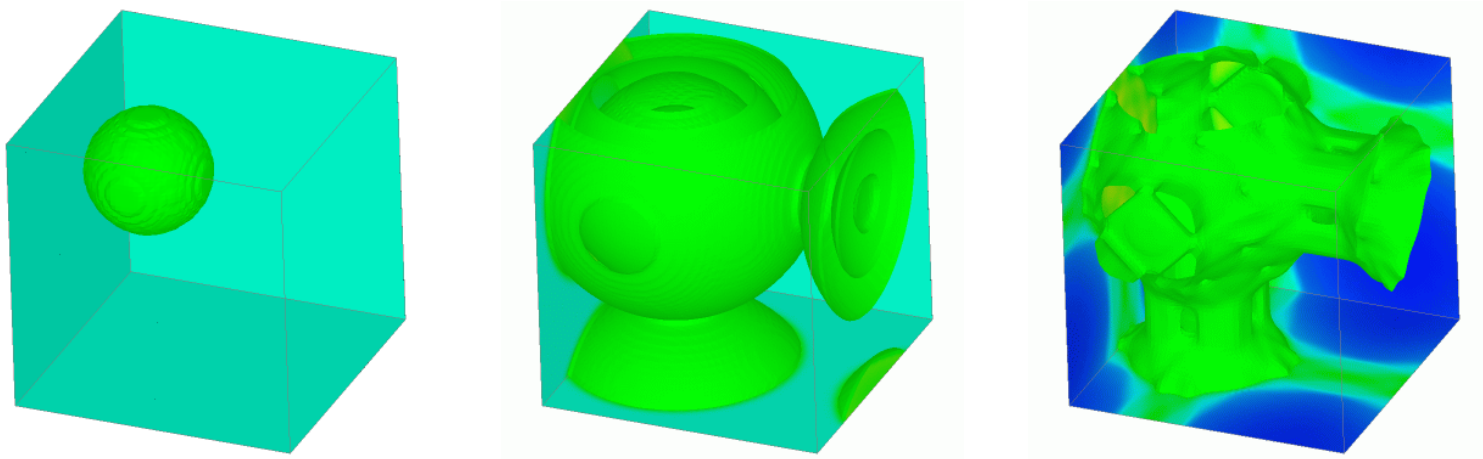

Evolution of density at $t = 0, t = 0.21$ and $t = 0.84$ (from left to right).

Source: amroc.sourceforge.net/examples/euler/3d/html.

In collaboration with Ralf Deiterding, Oak Ridge, USA

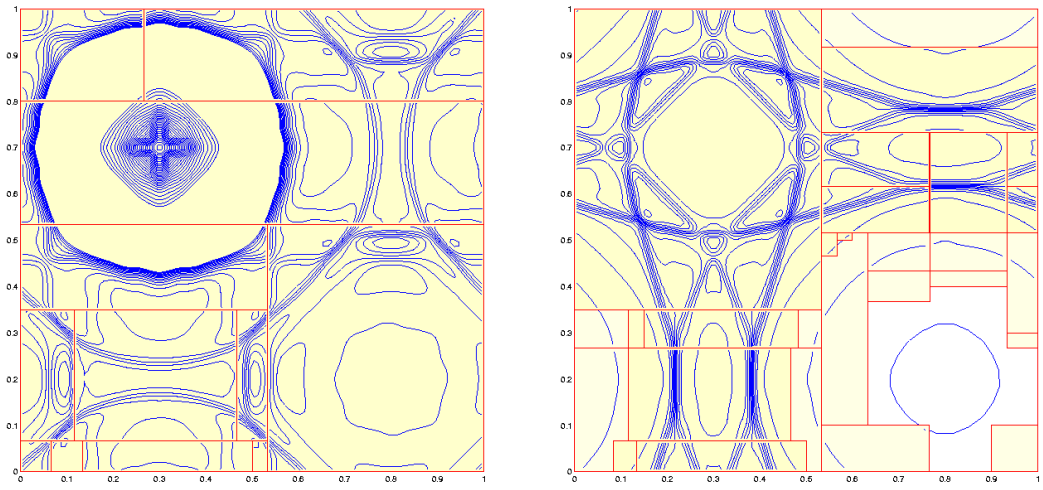

Evolution of the density solution, adaptive computations with 3 levels and 2 buffer cells.

Cut at $z = 0$ and $z = 0.5$ at time $t = 0.84$ (from left to right) .

Source: amroc.sourceforge.net/examples/euler/3d/html.

In collaboration with Ralf Deiterding, Oak Ridge, USA

Reaction-diffusion equations

2D thermo-diffusive flames

3D flame balls

Governing equations

Non-dimensional thermodiffusive equations

$$\partial_t T + \vec{v}\cdot\vec{\nabla}T - \nabla^2 T = \omega - s \quad (1)$$

$$\partial_t Y + \vec{v}\cdot\vec{\nabla}Y - \frac{1}{Le}\nabla^2 Y = -\omega \quad (2)$$

$$\omega(T,Y) = \frac{Ze^2}{2\,Le} Y \exp\left[\frac{Ze(T-1)}{1+\alpha(T-1)}\right] \text{ (reaction rate)}$$

$$s(T) = \gamma\left[\left(T+\alpha^{-1}-1\right)^4 - \left(\alpha^{-1}-1\right)^4\right] \text{ (heat loss due to radiation)}$$

+ initial and boundary conditions

$$Y = Y_1,\ T = \frac{\bar{T}-\bar{T}_u}{\bar{T}_b-\bar{T}_u},\ Le = \frac{\kappa}{D} \text{ (Lewis)},\ \alpha = \frac{\bar{T}_b-\bar{T}_u}{\bar{T}_b},\ Ze = \alpha\frac{E_a}{RT_b} \text{ (Zeldovich)}$$

$\vec{v}$ given by the incompressible NS equations. When the fluid is at rest, $\vec{v} = \vec{0}$.

Governing equations

Planar flames

- Flame propagation at the velocity v_f
- When the fresh mixture is advected at $v = -v_f \Rightarrow$ **steady planar flame**

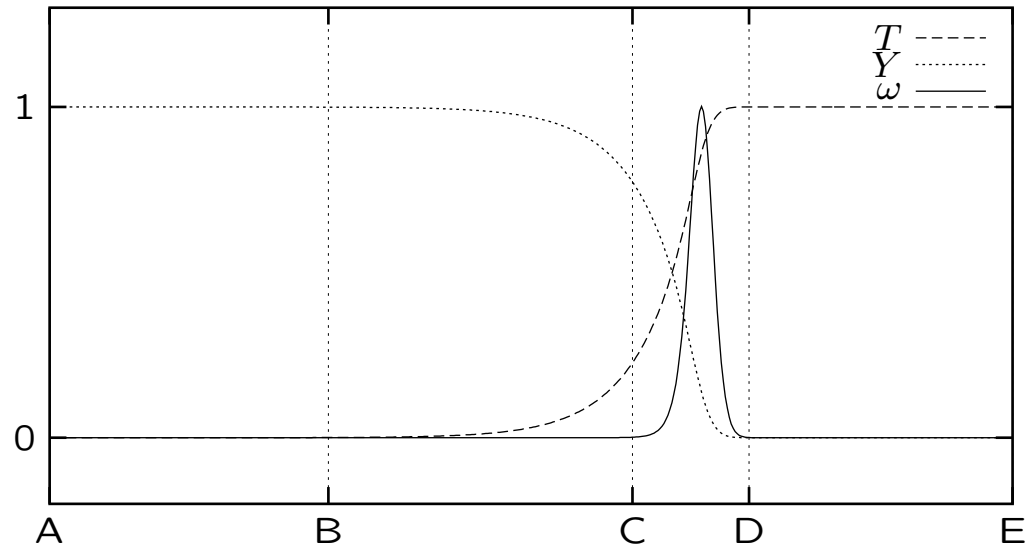

AB: *fresh mixture*, BC: *preheat zone*, CD: *reaction zone* $d = O(Ze^{-1})$, DE: *burnt mixture*

Governing equations

Thermodiffusive instability

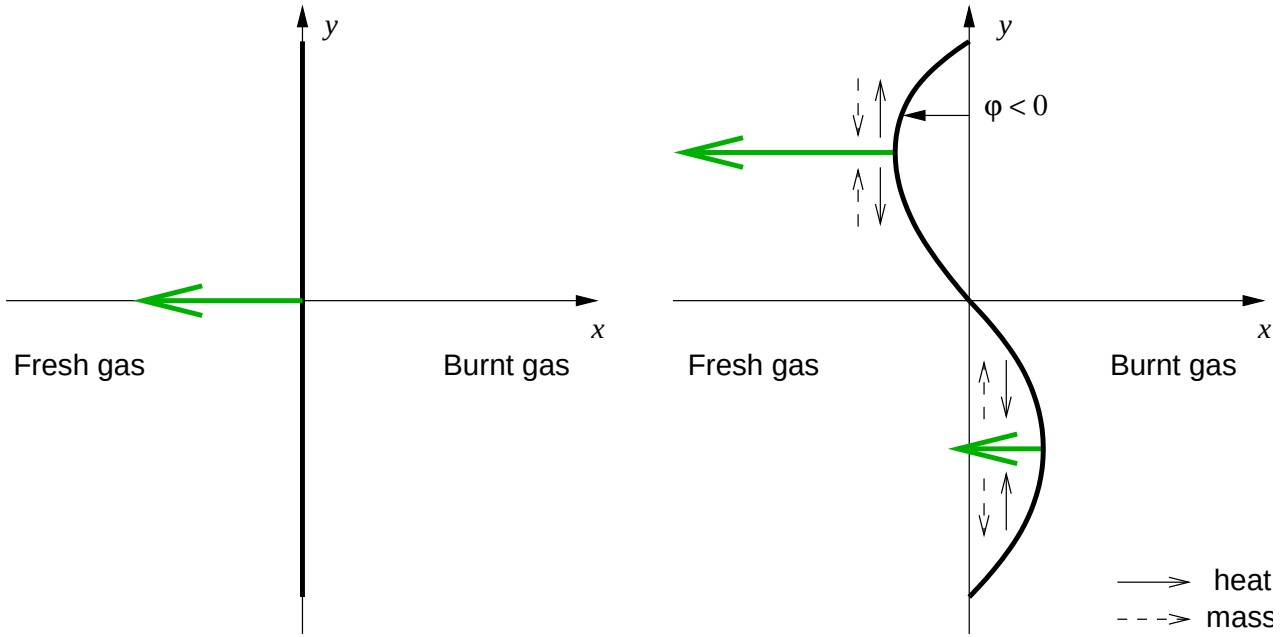

Stable: ω for $Le = 1$, $Ze = 10$ (animation) - Unstable: ω for $Le = 0.3$, $Ze = 10$ (animation)

Asymptotic theory for $Ze >> 1$ (Sivashinsky 1977, Joulin-Clavin 1979)

1) $Ze(Le-1) < -2$: cellular flames 2) $Ze(Le-1) > 16$: pulsating flames

2D Flame front

Temperature Reaction rate Adaptive grid

stable
Le = 1.0

Unstable
Le = 0.3

Application to TD flames

The flame ball configuration

- Simplest experiment to study the interaction of chemistry and transport of gases (experimental: Ronney 1984, theory: Buckmaster-Joulin-Ronney 1990-91)

- Enables to study the flammability limit of lean gaseous mixtures

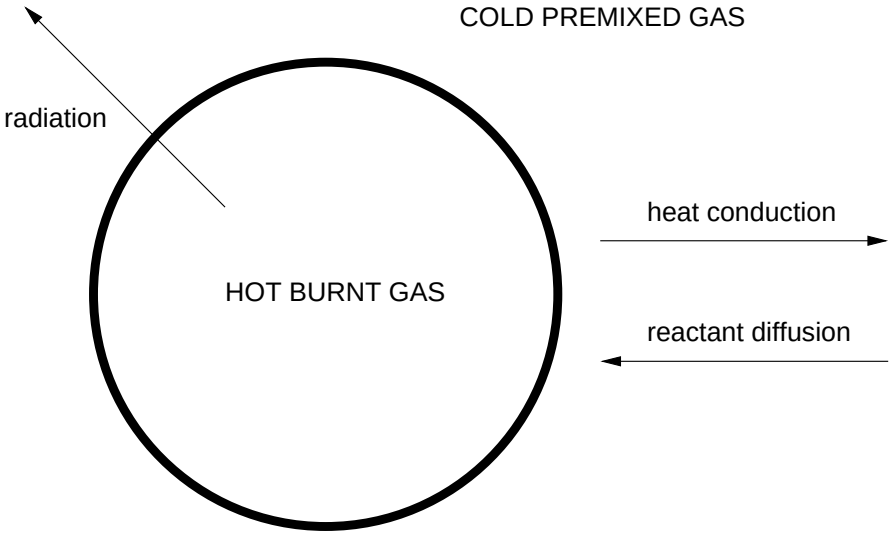

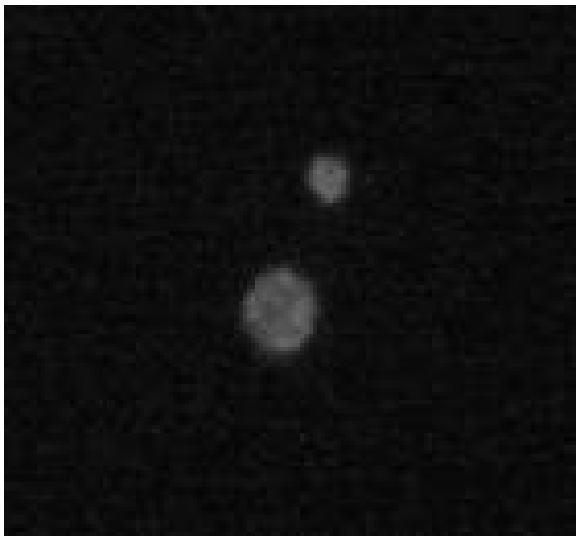

- Problem: the combustion chamber is finite $\Rightarrow$ **Interaction with wall**

Application to TD flames

Interaction flame front-adiabatic wall: the 1D case

- Lean mixture H_2-air, $Ze = 10$, $\alpha = 0.64$, $\Omega = [0, 30]$
- Radiation neglected
- Adiabatic walls $\Rightarrow$ Neuman boundary conditions
- Objective: study the inflence of Le
- Profiles of T and ω for $Le = 0.3$ (animation 1)
- Profiles of T and ω for $Le = 1$ (animation 2)
- Profiles of T and ω for $Le = 1.4$ (animation 3)

Ref. Roussel, Schneider, CTM 10 (2006)

Application to TD flames

Interaction flame front-adiabatic wall: the 1D case

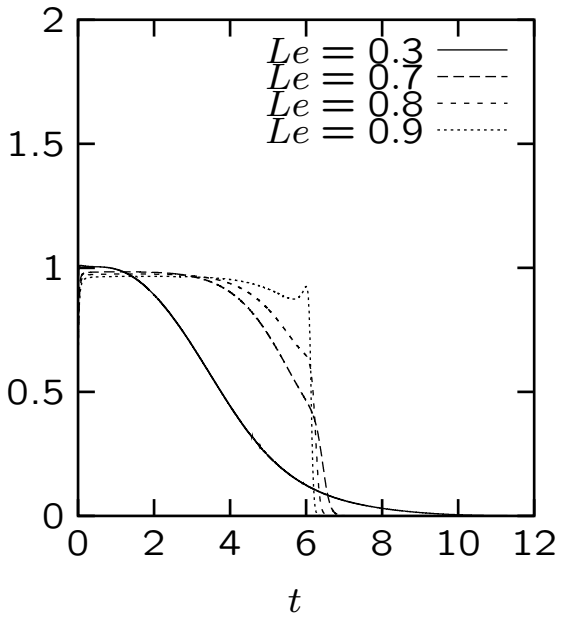

Flame velocity v_f for $Le < 0.95$

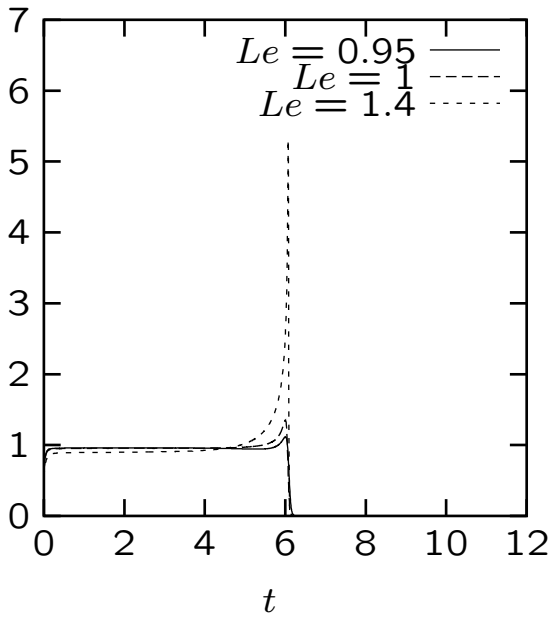

Flame velocity v_f for $Le \geq 0.95$

Ref. Roussel, Schneider, CTM 10 (2006)

Application to TD flames

Interaction flame ball-adiabatic wall

- Radiation neglected, $Ze = 10$, $\alpha = 0.64$, $\Omega = [-50, 50]^d$
- Adiabatic walls $\Rightarrow$ Neuman boundary conditions
- At $t = 0$, the radius of the flame ball is $r_0 = 2$.
- 2D: Evolution of T and mesh for $Le = 0.3$ (animations 1-2)
- 2D: Evolution of T for $Le = 1$ (animation 3)
- 2D: Evolution of T for $Le = 1.4$ (animation 4)
- 3D: Evolution of T and mesh for $Le = 1$ (animations 5-6)
- Analogy with capillarity for a fluid droplet

Ref. Roussel, Schneider, CTM 10 (2006)

Application to TD flames

Interaction flame ball-adiabatic wall

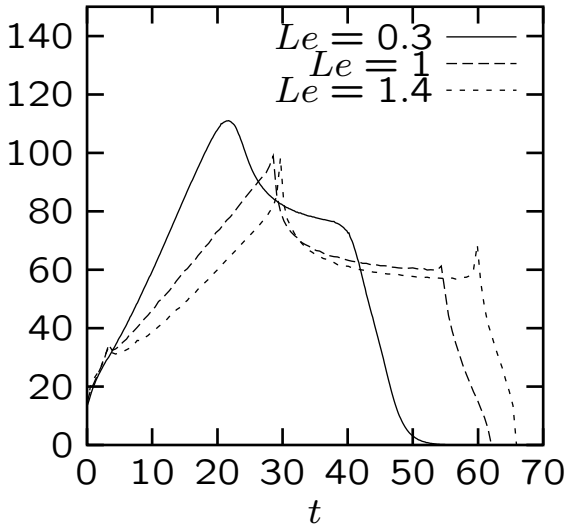

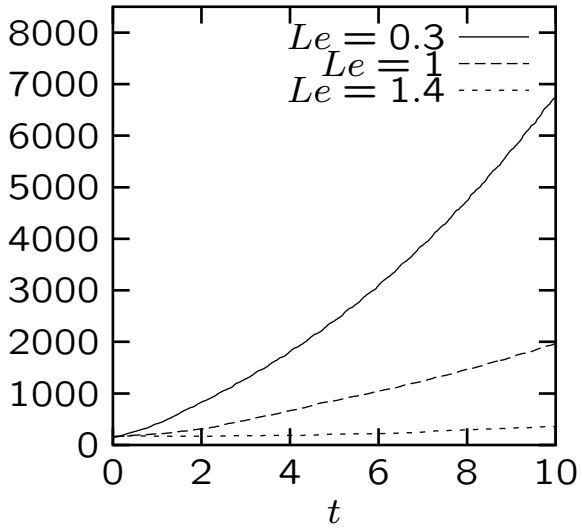

$\mathcal{R} = \int \omega \, d\Omega$ in 2D

$\mathcal{R} = \int \omega \, d\Omega$ in 3D

Ref. Roussel, Schneider, CTM 10 (2006)

Application to TD flames

Interaction flame ball-adiabatic wall: Performances

d	Le	$N_{\max}$	% CPU	% Mem
2	0.3	256^2	25.50%	14.10%
2	1	256^2	21.50%	11.75%
2	1.4	256^2	21.00%	11.10%
3	1	128^3	12.98%	4.38%

Application to TD flames

Interaction flame ball-vortex

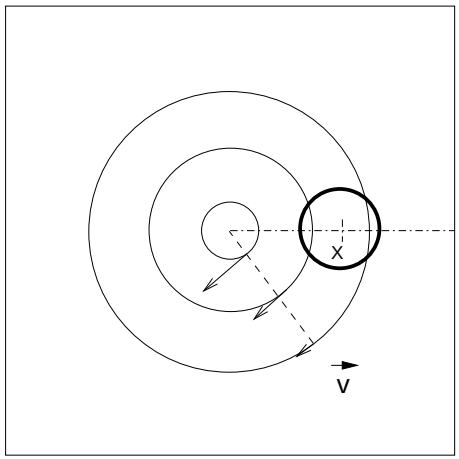

- Phenomenon which happens e.g. in furnaces
- Thermodiffusive model, $\vec{v}$ analytic solution of Navier-Stokes
- Evolution of T and mesh for $Ze = 10$, $Le = 0.3$, no radiation (animations)

Application to TD flames

Interaction flame ball-vortex

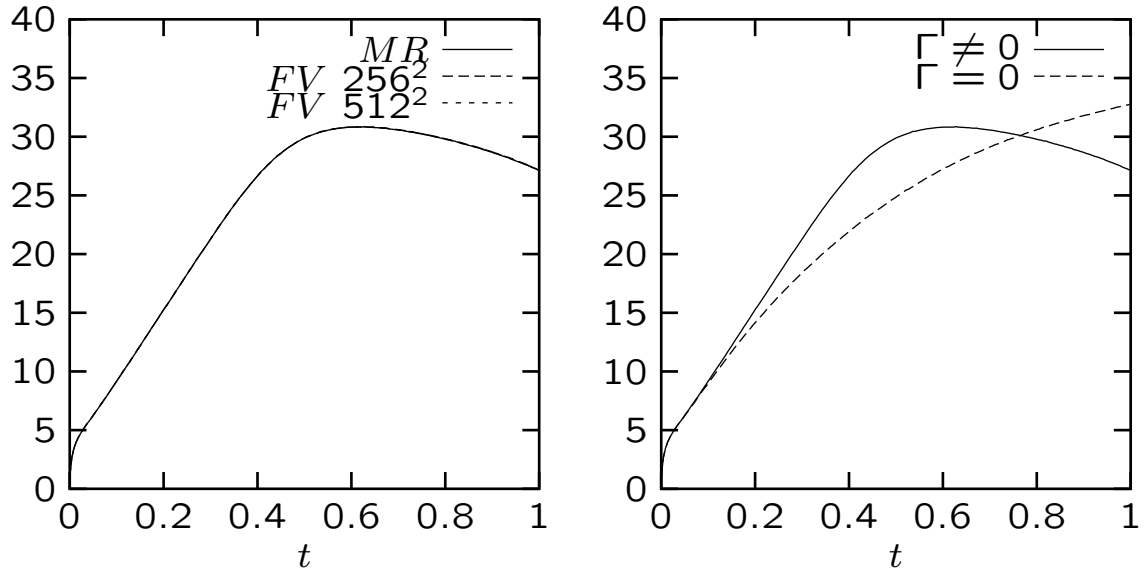

$\mathcal{R} = \int \omega \, d\Omega$: for MR and FV methods with and without vortex

Ref. Roussel, Schneider Comp. Fluids 34 (2005)

3D flame ball, Le = 1

Temperature

Adaptive grid

Splitting flame ball computed with the MR/LTS method

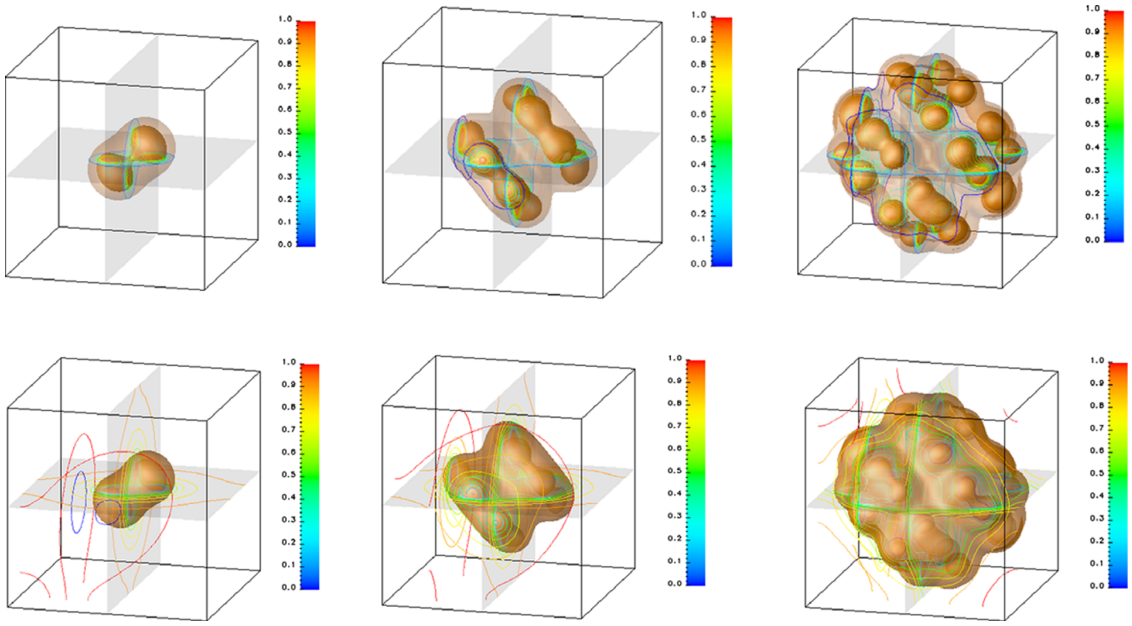

Temperature Concentration grid xy grid yz

Iso-surfaces and isolines on the cut-plane for temperature (top) and concentration (bottom) with L=8 scales, Le=0.3, Ze=10,k=0.1.

Ref. Domingues Gomes, Roussel and Schneider. JCP 227 (2008)

Splitting flame ball: projections of the cell centers used on the adaptive mesh

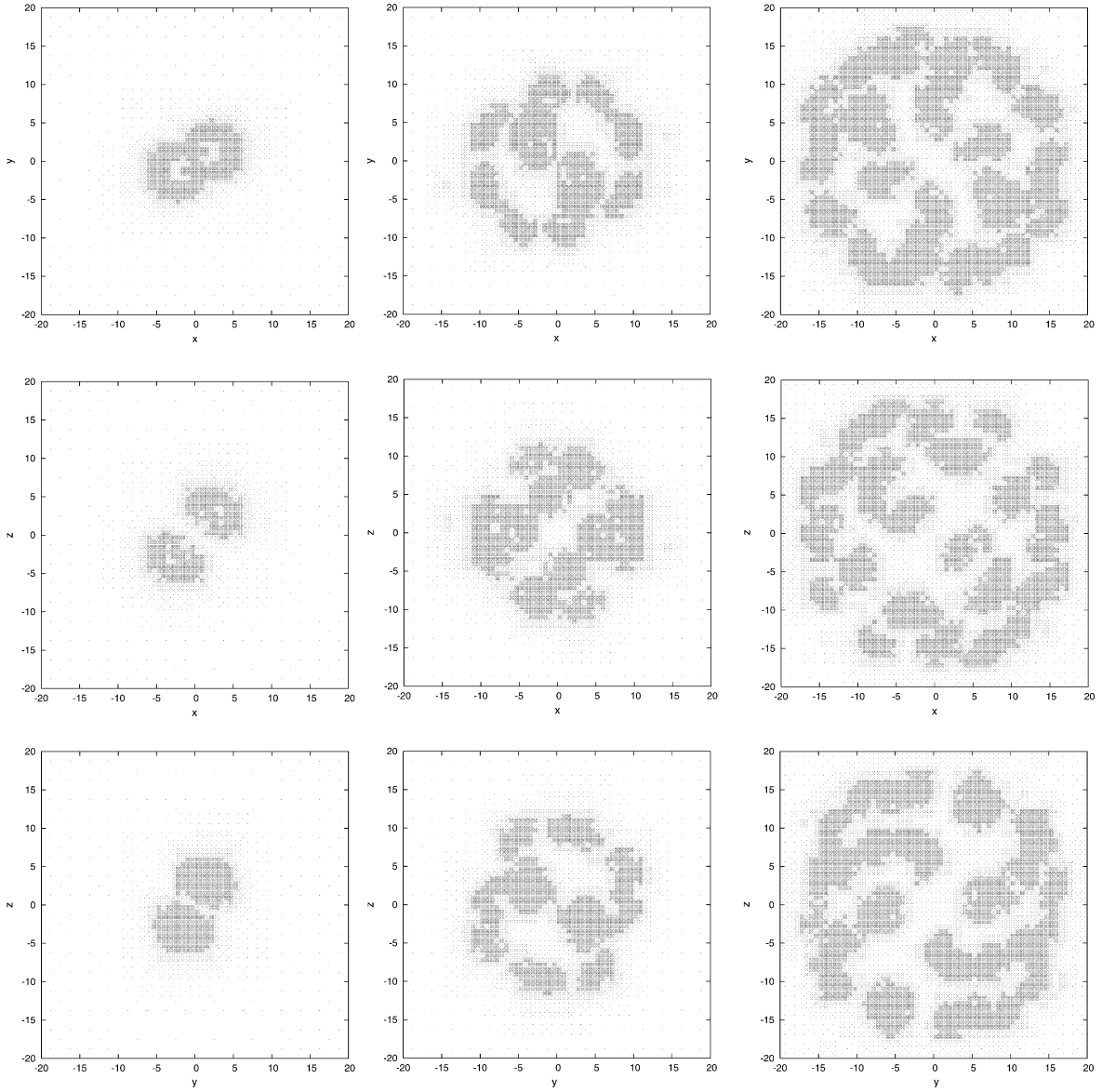

Ref. Domingues Gomes, Roussel and Schneider. JCP 227 (2008)

Splitting flame ball: CPU and memory compressions for the different methods with L=8 scales

Method	% CPU time	% Memory	Integral reaction rate
MR	2.7	1.05	669.09
MR/LTS	2.3	1.05	669.11

Ref. Domingues Gomes, Roussel and Schneider. JCP 227 (2008)

Conclusions

- Finite volume discretization with explicit time integration (both of second-order) to solve evolutionary PDEs in Cartesian geometry.
- Efficient space-adaptive multiresolution method (MR) with local time stepping (LTS). CPU speed-up and memory reduction, while controling the accuracy.
- Further speed-up due to an improved time advancement using larger time steps on large scales without violating the stability condition of the explicit scheme.
- However, synchronization of the tree data structure necessary.
- Time-step control (CTS) for space adaptive schemes (embedded Runge-Kutta schemes) and combination with LTS.
- Applications to reaction-diffusion equations, compressible Euler and Navier-Stokes equations.
- Next: develop level dependent time step control which allows to adapt the time step within a cycle of the level dependent time stepping MR/LTS.

http://www.cmi.univ-mrs.fr/~kschneid http://wavelets.ens.fr